

# ULRR

## Calorimetric determination of cocrystal thermodynamic stability: sulfamethazine–salicylic acid case study

Item Type	Article
Authors	Svärd, Michael; Ahuja, Dipali; Rasmuson, Åke C.
Citation	Crystal Growth & Design; 20 (7), pp.4243-4251
Publisher	American Chemical Society
Download date	2026-03-13 05:20:32
Item License	<a href="https://creativecommons.org/licenses/by-nc-sa/1.0/">https://creativecommons.org/licenses/by-nc-sa/1.0/</a>
Link to Item	<a href="https://hdl.handle.net/10344/8958">https://hdl.handle.net/10344/8958</a>

## Calorimetric Determination of Cocrystal Thermodynamic Stability: Sulfamethazine–Salicylic Acid Case Study

Michael Svård,\* Dipali Ahuja, and Åke C. Rasmuson

Cite This: <https://dx.doi.org/10.1021/acs.cgd.9b01253>

Read Online

ACCESS |



Metrics &amp; More

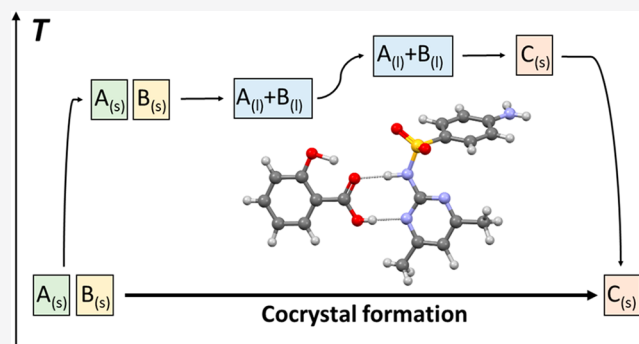


Article Recommendations



Supporting Information

**ABSTRACT:** This work demonstrates how the thermodynamics of cocrystal formation from the pure, solid cofomers can be directly determined from experimentally obtained calorimetric data, without involving solubility data or approximations of ideal solution. For the 1:1 cocrystal between the drug API sulfamethazine and salicylic acid, the melting temperatures and associated enthalpies of fusion have been determined for the cofomers in their respective pure solid state and as an equimolar physical mixture and for the cocrystal, using differential scanning calorimetry. Heat capacities have been determined for the respective solid forms and their supercooled melts. The Gibbs energy for cocrystal formation and the enthalpic and entropic components have been determined as functions of temperature through a thermodynamic cycle. The Gibbs energy, enthalpy, and entropy of mixing have been estimated from the thermodynamic functions for cocrystal formation and fusion of the solid phases. The results show that the Gibbs energy for cocrystal formation is negative, i.e. the cocrystal is the stable solid phase in relation to a 1:1 mixture of the cofomers throughout the temperature interval from room temperature to the cocrystal melting point, and becomes increasingly negative with increasing temperature. Cocrystal formation is an endothermic process, driven by the favorable entropy increase, and is accompanied by a 6% increase in molecular volume. At room temperature, liquid mixing of cofomers is found to be weakly exothermic. The results qualitatively align with a previously reported analysis based on solubility data.



## 1. INTRODUCTION

As pharmaceutical compounds with poor aqueous solubility are becoming increasingly common, methods for improving the pharmacokinetics of these kinds of drugs without affecting the molecular composition are gaining in importance. Physicochemical properties that affect the efficiency and stability of an active pharmaceutical ingredient include the solubility behavior, dissolution rate, and thermal stability, as well as properties such as compressibility and hygroscopicity.<sup>1</sup> Conventional ways to improve these properties are salt formation, solubilization, complexation, and micronization.<sup>2</sup> Multicomponent crystals (cocrystals) offer an alternative path with significant benefits, including the potential to increase aqueous solubility and fine-tune the solubility behavior and other important properties through judicious cofomer selection.<sup>3</sup> The cocrystal approach can also offer opportunities to exploit intellectual property rights.

As a consequence, gradually more importance is attached to discovering new cocrystal formulations, also for APIs already on the market. Recent international guidelines define a cocrystal as a solid, crystalline material composed of two or more molecules in the same crystal lattice.<sup>4</sup> Part of a continuum of multicomponent solid phases, also containing salts and solvates, a proposed definition of a true cocrystal is

that its structure contains a stoichiometric ratio of electrically neutral molecules whose pure components are solids at room temperature and pressure.<sup>5</sup> Cocrystals can be manufactured by many different methods. The most common is crystallization from solution involving cooling or a gradual adjustment of the solvent composition,<sup>1,6,7</sup> while other methods including grinding, evaporation crystallization, and spray-drying.<sup>8–11</sup>

Despite the surge in popularity and the accompanying increase in publications reporting new cocrystal systems, comparatively little has been reported on the various thermodynamic aspects of cocrystals in relation to the solid cofomers, which are key to understanding their formation, as well as their stability and dissolution behavior in solution. In the present work, the thermodynamics of formation of a 1:1 cocrystal between sulfamethazine and salicylic acid from its solid components have been explored in depth, by the

Received: September 20, 2019

Revised: June 2, 2020

Published: June 4, 2020



application of differential scanning calorimetry. Sulfamethazine (SMT), also known as sulfadimidine, is a sulfonamide drug with antimicrobial and anti-infective properties,<sup>12,13</sup> whose bioavailability is limited by its low solubility. SMT has one known crystal structure<sup>14</sup> but in analogy with many other sulfa drugs has shown a strong propensity to form cocrystals,<sup>13,15</sup> including a 1:1 cocrystal with the coformer salicylic acid (SA) (Figure 1).

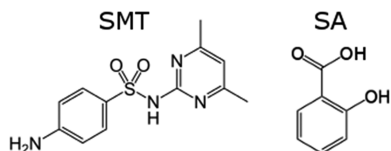


**Figure 1.** Molecular structure of sulfamethazine (SMT, left) and salicylic acid (SA, right).

## 2. THEORY

Consider a cocrystal C, formed from  $a$  moles of coformer A and  $b$  moles of coformer B:



For a 1:1 cocrystal,  $a = b = 1$ . The property determining the relative stability of a cocrystal in relation to its coformers is the Gibbs energy change of the reaction in eq 1. In the following, according to the established terminology for multicomponent solids,<sup>17–21</sup> this is termed the Gibbs energy for cocrystal formation,  $\Delta_{\text{form}}G_C$ . This property is generally defined for the process in eq 1 with both reactants and product in the solid state at temperature  $T$ :

$$\Delta_{\text{form}}G_C = \Delta_{\text{form}}H_C - T\Delta_{\text{form}}S_C = G_C^s - G_A^s - G_B^s \quad (2)$$

Like all Gibbs energy changes,  $\Delta_{\text{form}}G_C$  has an enthalpic ( $\Delta_{\text{form}}H_C$ ) and an entropic ( $T\Delta_{\text{form}}S_C$ ) component. A negative  $\Delta_{\text{form}}G_C$  signifies that the total process of mixing equal parts of the solid coformers at a molecular level and forming the cocrystal structure is thermodynamically favored and is spontaneous. This process can be envisaged as breaking the crystal structures A and B to form a supercooled melt, from which C is subsequently crystallized (solvent-free path), or alternatively the dissolution of equal parts A and B into a solution with a composition corresponding to saturation with respect to C, followed by crystallization of C to restore equilibrium (solution path).

The relative stability of a cocrystal in relation to its coformers can be estimated in a number of ways. In an approximate approach, relative lattice energies of cocrystals and their crystalline components may be compared. This offers a method to computationally predict the occurrence of cocrystals.<sup>22,23</sup> However, a method based on lattice energies neglects the influence of entropy on the propensity for cocrystal formation, and moreover, computational methods for calculation of lattice energies often neglect zero-point energies as well as thermal effects.<sup>24,25</sup>

$\Delta_{\text{form}}G_C$  can also be estimated experimentally using solubility data.<sup>26–29</sup> By setting the reference state for the chemical potentials to the respective solid phases, an expression for the Gibbs energy for cocrystal formation in terms of activities of A and B in solution can be obtained, as shown in eq 3

$$\Delta_{\text{form}}G_C = -RT \ln \frac{(a_A^+)^a (a_B^+)^b}{(a_A)^a (a_B)^b} \quad (3)$$

where  $a_A^+$  and  $a_B^+$  denote the activities of A and B in the saturated solutions of pure A and pure B, respectively, and  $a_A$  and  $a_B$  are the activities in a solution at equilibrium with a 1:1 cocrystal. Neglecting the influence of activity coefficients on the solubility—a routinely used approximation which is strictly only valid for ideal solutions and dilute solutions obeying Henry's law—results in an expression in terms of the solubility,  $c_{\text{eq}}$  of the pure components A and B

$$\Delta_{\text{form}}G_C \approx -RT \ln \frac{(c_{\text{eq,A}})^a (c_{\text{eq,B}})^b}{K_s} \quad (4)$$

where  $K_s$  denotes the solubility product for a solution at equilibrium with the cocrystal,  $c_A^a c_B^b$ .<sup>30</sup> For the case of a 1:1 cocrystal, eqs 3 and 4 reduce to

$$\Delta_{\text{form}}G_C = -RT \ln \frac{a_A^+ a_B^+}{a_A a_B} \approx -RT \ln \frac{c_{\text{eq,A}} c_{\text{eq,B}}}{K_s} \quad (5)$$

Finally,  $\Delta_{\text{form}}G_C$  and its components could be estimated on the basis of calorimetric data. Zhang et al.<sup>19,24</sup> determined enthalpies for the formation of several cocrystals using differential scanning calorimetry and back-calculated the entropy term using  $\Delta_{\text{form}}G_C$  obtained from solubility data. Oliveira et al.<sup>21</sup> used data on the enthalpy of solution to calculate enthalpies for cocrystal formation for several saccharin-based cocrystals and then obtained  $\Delta_{\text{form}}G_C$  using solubility data. Perlovich<sup>31</sup> estimated Gibbs energies for cocrystal formation by correlating melting temperatures and Gibbs energies of sublimation. Braun et al.<sup>32</sup> estimated  $\Delta_{\text{form}}G_C$  of a crystalline racemic compound of naproxen from a racemic conglomerate from calorimetric melting data. However, it appears no study has yet been published in the open literature reporting a full experimental determination of  $\Delta_{\text{form}}G_C$  of a cocrystal composed of chemically different molecules solely on the basis of differential scanning calorimetry data, and moreover no study has reported a calorimetry-based determination of  $\Delta_{\text{form}}G_C$  which specifically accounts for the contributions from heat capacity.

## 3. EXPERIMENTAL WORK

Solid sulfamethazine (CAS registry no. 57-68-1, nominal purity >99%) and salicylic acid (CAS registry no. 69-72-7, nominal purity >99%) were purchased from Sigma-Aldrich and used with no further purification. The 1:1 cocrystal was synthesized using solvent drop grinding as described in a previous publication.<sup>33</sup> The solid materials were characterized by X-ray powder diffraction (XRPD) using an Empyrean diffractometer (PANalytical, Philips) with Cu  $K\alpha_{1,2}$  radiation at 40 kV and 40 mA and verified to be identical with the only previously described crystalline phases of the respective compounds<sup>14,16,34</sup> (XRPD patterns are provided as Supporting Information). A 1:1 molar ratio physical mixture of the two pure solid coformers (SMT and SA) was prepared by careful weighing and gentle mixing of equimolar amounts of separately ground crystal powders.

The melting temperature,  $T_m$ , and the associated enthalpy of fusion,  $\Delta_{\text{fus}}H$ , of solid sulfamethazine, the 1:1 salicylic acid–sulfamethazine cocrystal, and a 1:1 physical mixture of the two pure solid coformers have been determined by differential scanning calorimetry (DSC). Measurements were carried out on a TA Instruments Q2000 instrument, using a constant heating rate of 3 K  $\text{min}^{-1}$ . The heat capacity of the solid states,  $C_p^s$ , and melts,  $C_p^l$ , of

Table 1. DSC Data for the Solid Phases and Their Respective Melts, Together with Coefficients of Eq 6<sup>a</sup>

	sulfamethazine	salicylic acid	1:1 cocrystal	1:1 physical mixture
Melting Point				
$T_m/K$ [N]	$469.66 \pm 0.08$ [4]	$431.35 \pm 0.35^{35}$ [14]	$469.52 \pm 0.13$ [4]	$426.05 \pm 0.17$ [4]
$\Delta_{\text{fus}}H(T_m)/\text{kJ mol}^{-1}$	$36.0 \pm 0.44$	$27.09 \pm 0.17^{35}$	$60.3 \pm 1.8$	$63.5 \pm 1.6$
$\Delta_{\text{fus}}S(T_m)/\text{J K}^{-1} \text{mol}^{-1}$	$76.7 \pm 0.95$	$62.8 \pm 0.36^{35}$	$128 \pm 3.8$	$149 \pm 3.8$
Specific Heat Capacity				
$k^s/\text{J K}^{-2} \text{mol}^{-1}$	0.9057	0.5248	1.4309	-
$m^s/\text{J K}^{-1} \text{mol}^{-1}$	46.32	10.49	118.10	-
$k^l/\text{J K}^{-2} \text{mol}^{-1}$	0.3051	0.5884		0.8015
$m^l/\text{J K}^{-1} \text{mol}^{-1}$	439.40	48.40		576.73
$T$ range (s)/K [N]	278–455 [5]	273–418 [4]	280–438 [4]	-
$T$ range (l)/K [N]	416–467 [4]	418–432 [4]		423–468 [4]

<sup>a</sup>Experimental data are given together with expanded standard uncertainties at the 95% confidence level, obtained from standard errors over  $N$  repeat experiments.

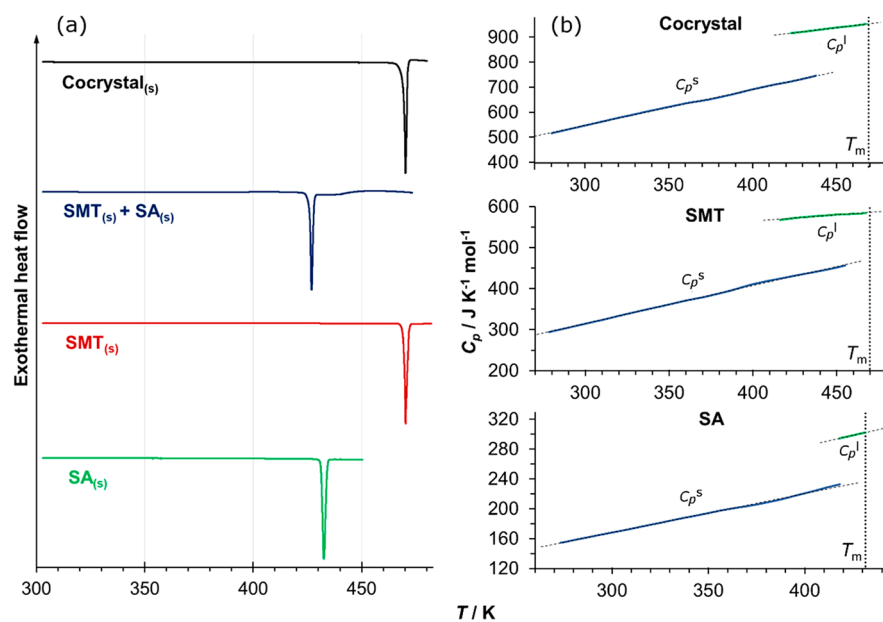


**Figure 2.** (a) DSC thermograms showing melting endotherms of the cocrystal, the equimolar physical mixture of cofomers, and the pure cofomers. (b) Heat capacities of the solids and supercooled melts of the cocrystal and the pure cofomers together with linear fits.

salicylic acid, sulfamethazine, and the 1:1 cocrystal have been determined by temperature-modulated DSC, using a TA Instruments Q2000 instrument. A modulation period of 100 s, an amplitude of 1 K, and a constant underlying heating rate of 5 K min<sup>-1</sup> were used; these conditions were established as optimal on the basis of preliminary experiments. Heat capacity data for the solid forms were collected in an initial heating step. After melting, the heat capacity of the respective supercooled melts were then obtained in a second heating step, following a rapid cooling of the pans containing the melts to a point below the melting temperature but above the temperatures where recrystallization would occur.

In all DSC experiments, evenly distributed powder samples of approximately 5 mg were encapsulated in Tzero aluminum pans. The furnace was purged with nitrogen gas at 50 mL min<sup>-1</sup>. The instrument was calibrated for data collection on heating against the melting properties of indium, and the heat capacity signal was calibrated using sapphire, with a linear function of heat capacity vs temperature. Differences in mass between the sample and reference pans were restricted to  $\leq 0.20$  mg in all runs.

Thermogravimetric analysis (TGA) was carried out on the three pure solid phases using a TA Instruments Q50 instrument. The furnace was purged with nitrogen gas, and powder samples were placed in platinum pans and heated to 770 K at a constant heating rate of 10 K min<sup>-1</sup>.

## 4. RESULTS

The extrapolated onset melting temperature and the associated enthalpy of fusion of sulfamethazine, the 1:1 cocrystal, and the 1:1 physical mixture have been determined, each as averages of four repeat DSC runs. The data are given in Table 1 together with data for salicylic acid,<sup>35</sup> and representative thermograms are shown in Figure 2a. The thermogram for the physical mixture shows a clear endotherm at a temperature significantly below that of the cocrystal, with some weak residual endothermic activity extending after the peak. There is no trace of a melting peak corresponding to the cocrystal in this thermogram, which indicates complete melting of the physical mixture without transformation into the cocrystal.

The thermograms of all samples show straight baselines up to the respective melting endotherms, indicating that no phase transformation occurred in any of the samples prior to melting. Reweighing of the sample pans run confirmed that the sample mass was unchanged after each run. The TGA traces (available as Supporting Information) show no measurable mass loss, indicating that the samples were completely dry, until the onset of melting for SMT, with a gradual mass decrease starting

slightly prior to melting for SA and the cocrystal, corresponding to sublimation in the open pan environment.

The specific heat capacities of the pure solid forms and their respective melts over a range of temperatures have been determined as averages of four to five repeat DSC runs, and fitted to a linear equation of two parameters  $k$  and  $m$ :

$$C_p(T) = kT + m \quad (6)$$

As shown in Figure 2b, the  $C_p(T)$  curves for all three solids and their respective melts are all to a good approximation linear over the recorded temperature intervals ( $R^2$  values exceeding 0.99 with the exception of the melt of sulfamethazine, for which  $R^2 = 0.97$ ). The coefficients  $k$  and  $m$  are given in Table 1 together with the temperature ranges of the experimental data. Please note that, with respect to the units for the cocrystal and the physical mixture, 1 mol consists of 1 mol of SMT and 1 mol of SA. The experimental data are given in the Supporting Information.

The heat capacity for the cocrystal exceeds the combined heat capacities of the cofomers throughout the evaluated temperature range, for both the solid and the melt; for the solids at room temperature, the difference is  $61 \text{ J K}^{-1} \text{ mol}^{-1}$ , or about 13%, and for the melts at the melting temperature of the cocrystal, the difference is  $46 \text{ J K}^{-1} \text{ mol}^{-1}$  (5%). Likewise, the enthalpy and entropy of fusion of the physical mixture exceeds the combined respective values of the cofomers, albeit at a different temperature.

## 5. EVALUATION AND DISCUSSION

**5.1. Estimating the Binary Phase Diagram of the System SMT–SA from DSC Data.** The thermogram of the 1:1 physical mixture in Figure 2a exhibits an endotherm composed of an initial main sharp peak followed by an extended weak tail of endothermic activity. This indicates that the composition of the physical mixture does not exactly correspond to the eutectic between SMT and SA. The main peak is caused by melting of the eutectic, and the residual tail is the gradual melting and mixing (i.e., dissolution) of the remaining pure component (SMT) along its liquidus curve. The absence of any exothermal activity and of any additional melting peak indicates that the melting is not accompanied by a recrystallization into the cocrystal.

By analysis of the DSC data, a tentative binary phase diagram of the system has been constructed (Figure 3). It is clear from the figure that the cocrystal exhibits congruent melting behavior and is the stable solid phase at an equimolar composition.

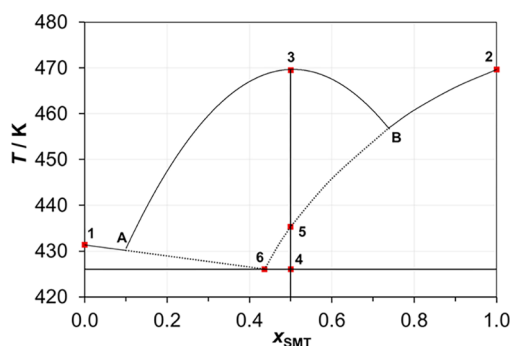


Figure 3. Phase diagram of the system SA–SMT.

The phase diagram is based on the experimentally determined points 1–4 and the estimated locations of points 5 and 6, as follows. Point 1 is the melting point of pure SA. Point 2 is the melting point of pure SMT. Point 3 is the congruent melting point of the 1:1 cocrystal. Point 4 is the melting temperature of the metastable eutectic between SA and SMT. For the determination of point 4, the extrapolated onset temperature of the main peak of the 1:1 physical mixture was taken. Point 5 is the intersection of the (metastable) liquidus of SMT at  $x = 0.5$ . For the location of point 5, the temperature has been estimated from the thermograms of the 1:1 physical mixture. The resulting value obtained is  $435.3 \pm 0.24 \text{ K}$ , which is 9.3 K above the eutectic temperature. Point 6 is the eutectic point. For the location of point 6, the composition was estimated on the basis of fractional integration of the collected thermograms of the 1:1 physical mixture, according to the principle of the lever arm rule. The area of the residual part of the peak is compared to the total area, with the areas weighted using the pure component enthalpies of fusion (of pure SMT and of the 1:1 mixture, respectively—this treatment entails assuming that the contributions from differences in liquid mixing can be neglected). The resulting value obtained is  $x_{\text{SMT}} = 0.44$ .

The liquidus of SMT has been estimated on the basis of points 2, 5, and 6, and the liquidus of SA is plotted as a line from point 1 to point 6. Please note that the curvature of the liquidus of the cocrystal has not been determined, and the line shown in Figure 3 is only a schematic. Points A and B represent the intersections of the liquidus of the cocrystal with the respective liquidi of the pure components, and the locations of these points have not been determined.

**5.2. Estimating the Gibbs Energy for Cocrystal Formation from DSC Data.** Estimation of the thermodynamic functions of cocrystal formation from solid components can be accomplished indirectly by analysis of a path in a suitable thermodynamic cycle. A complete thermodynamic cycle for the solvent-free path from solid A + solid B to solid C at temperature  $T$  is depicted in Figure 4 for a 1:1 cocrystal. This cycle takes into account phase transitions, mixing and heat capacity contributions.

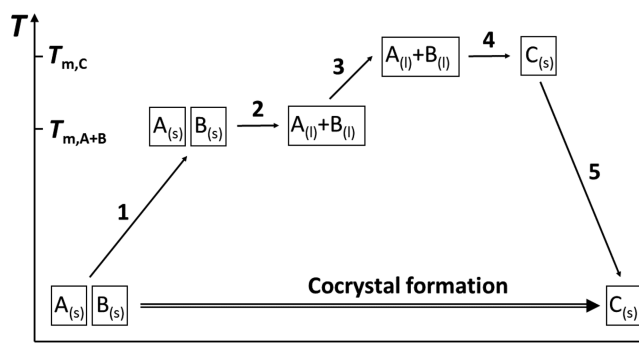


Figure 4. Thermodynamic cycle for cocrystal formation.

With reference to Figure 4, step 1 is the heating of a physical mixture of stoichiometrically correct proportions of the solid cofomers to the melting temperature of the physical mixture,  $T_{m,A+B}$ , where the mixture melts, step 2. Step 3 is the heating of the molten mixture to the melting temperature of the cocrystal C. Step 4 is the crystallization of C from the melt at the melting point of the cocrystal, and step 5 is the subsequent

cooling of solid cocrystal C back to the starting temperature. If the composition of the physical mixture corresponds to the eutectic,  $T_{m,A+B}$  is equal to the eutectic temperature. At this temperature, melting would then be accompanied by a simultaneous liquid mixing of A and B molecules, contributing to both the enthalpy change and the entropy change of the total phase transition from solid to liquid, step 2. However, if as in the current case the composition of the physical mixture, and hence the cocrystal, differs from the eutectic composition, melting and mixing of the eutectic will occur at the eutectic temperature until one of the components is consumed, and with further heating the remainder of the other component (in this case SMT) will gradually melt and mix (dissolve) into the solution until the system composition corresponds to the liquidus of this component (cf. point 5 in Figure 3).

The Gibbs energy change for the process as outlined in Figure 4 is  $\Delta_{\text{form}}G_C = \Delta_{\text{form}}H_C - T\Delta_{\text{form}}S_C$ . The total changes in enthalpy,  $H$ , and entropy,  $S$ , for steps 1 through 5 become

$$\begin{aligned} \Delta_{\text{form}}H_C(T) = & \underbrace{\int_T^{T_{m,A+B}} (C_{p,A}^s + C_{p,B}^s) dT}_1 \\ & + \underbrace{\frac{\Delta_{\text{fus+mis}}H_{A+B}(T_{m,A+B})}{2}}_2 + \underbrace{\int_{T_{m,A+B}}^{T_{m,C}} C_{p,C}^l dT}_3 \\ & - \underbrace{\frac{\Delta_{\text{fus}}H_C(T_{m,C})}{4}}_4 + \underbrace{\int_{T_{m,C}}^T C_{p,C}^s dT}_5 \end{aligned} \quad (7)$$

$$\begin{aligned} \Delta_{\text{form}}S_C(T) = & \underbrace{\int_T^{T_{m,A+B}} \left( \frac{C_{p,A}^s}{T} + \frac{C_{p,B}^s}{T} \right) dT}_1 \\ & + \underbrace{\frac{\Delta_{\text{fus+mis}}H_{A+B}(T_{m,A+B})}{T_{m,A+B}}}_2 + \underbrace{\int_{T_{m,A+B}}^{T_{m,C}} \frac{C_{p,C}^l}{T} dT}_3 \\ & - \underbrace{\frac{\Delta_{\text{fus}}H_C(T_{m,C})}{T_{m,C}}}_4 + \underbrace{\int_{T_{m,C}}^T \frac{C_{p,C}^s}{T} dT}_5 \end{aligned} \quad (8)$$

Since heat capacity data are frequently not available for all phases, the influence of the heat capacity terms in estimation of thermodynamic functions from DSC data is often neglected or simplified: e.g., approximated with a constant value such as the entropy of fusion at  $T_m$ .<sup>36</sup> However, the temperature dependence of the heat capacity can often be a significant contribution to the total temperature dependence of the enthalpy and entropy of a process and accordingly has to be adequately accounted for. In similarity to numerous other organic condensed phases,<sup>37,38</sup> the heat capacity curves of the phases considered in this work all to a good approximation exhibit a linear temperature dependence over the temperature ranges investigated. Assuming that this linear temperature dependence holds over the respective temperature ranges involved, the integrals in eqs 7 and 8 can be solved analytically using the coefficients in Table 1.

For steps 2 and 4, the experimentally determined values of the enthalpy and entropy are reported in Table 1. For steps 1, 3, and 5, the values of the integral terms are obtained by inserting the appropriate coefficients listed in Table 1 into eq 6 and solving. (A denotes sulfamethazine, ' salicylic acid, and C

the 1:1 cocrystal.) With respect to step 2, it is assumed that the melting and mixing occurs in a single step at the thermodynamic equilibrium temperature for the combined process. With respect to the heat-capacity-dependent steps 1, 3, and 5, it is assumed that the heat capacities depend linearly on temperature over the temperature ranges covered by the respective steps in Figure 4 and hence for the cocrystal that the linear temperature dependence can be extrapolated slightly outside the experimental temperature range. In this work, all heat capacities in eqs 7 and 8 have been shown to exhibit a clear linear temperature dependence over the respective range of experimental data, Figure 2 b, with  $R^2$  values exceeding 0.99.

For  $\Delta_{\text{form}}H_C$ :

$$\begin{aligned} \Delta_{\text{steps1+3+5}}H(T) &= \frac{k_A^s + k_B^s}{2} (T_{m,A+B}^2 - T^2) + (m_A^s + m_B^s) \\ & \quad (T_{m,A+B} - T) + \\ & \quad \frac{k_C^l}{2} (T_{m,C}^2 - T_{m,A+B}^2) + m_C^l (T_{m,C} - T_{m,A+B}) \\ & \quad + \frac{k_C^s}{2} (T^2 - T_{m,C}^2) + m_C^s (T - T_{m,C}) \end{aligned} \quad (9)$$

and for  $\Delta_{\text{form}}S_C$ :

$$\begin{aligned} \Delta_{\text{steps1+3+5}}S(T) &= (k_A^s + k_B^s) (T_{m,A+B} - T) + (m_A^s + m_B^s) \\ & \quad \ln \frac{T_{m,A+B}}{T} + \\ & \quad k_C^l (T_{m,C} - T_{m,A+B}) + m_C^l \ln \frac{T_{m,C}}{T_{m,A+B}} + k_C^s (T - T_{m,C}) \\ & \quad + m_C^s \ln \frac{T}{T_{m,C}} \end{aligned} \quad (10)$$

Estimated values of  $\Delta_{\text{form}}G_C$  and its enthalpic and entropic components at 298 K together with the respective contributions from the steps in Figure 4 are given in Table 2 for the 1:1

**Table 2. Gibbs Energy, Enthalpy, and Entropy for the Formation of the 1:1 Cocrystal at 298 K, Together with Terms of Eqs 7 and 8, with Uncertainties at the 95% Confidence Level**

step <sup>a</sup>	$\Delta H/\text{kJ mol}^{-1}$	$T\Delta S/\text{kJ mol}^{-1}$	$\Delta G/\text{kJ mol}^{-1}$
1	73.6 ± 1.6	60.6 ± 1.4	13.0 ± 0.29
2	63.5 ± 1.6	44.4 ± 1.1	19.1 ± 0.48
3	40.7 ± 0.91	27.1 ± 0.60	13.6 ± 0.30
4	-60.3 ± 1.8	-38.2 ± 1.1	-22.0 ± 0.65
5	-114.4 ± 2.6	-89.1 ± 2.0	-25.3 ± 0.56
total	3.1 ± 4.0	4.8 ± 2.9	-1.7 ± 1.1

<sup>a</sup>Relating to Figure 4 and eqs 7 and 8.

SMT-SA cocrystal. Estimated uncertainties are based on an analysis of the data, as expounded upon in the Supporting Information. Notably, because of the inherent correlation between the enthalpy and entropy terms (enthalpy–entropy compensation), the uncertainties of these terms are correlated, and consequently the uncertainty in the Gibbs energy becomes smaller than the uncertainties of the enthalpic and entropic component terms.

The approach for estimating the thermodynamic functions of cocrystal formation used here is dependent on a few key conditions and assumptions. One condition for using the thermodynamic cycle in Figure 4 is that the cocrystal does not form before or during melting of the physical mixture. This kind of behavior, which has been reported for other cocrystals in the literature,<sup>19,24</sup> seems to be promoted by a gentle treatment of component solids, in particular avoiding cogrinding,<sup>39</sup> but its occurrence is likely very system dependent.

Another assumption is that the equimolar physical mixture will melt completely in a single step, as it would at the eutectic composition. As shown in Figure 3 and discussed earlier, the eutectic composition ( $x_{\text{SMT}} = 0.44$ ) differs from the cocrystal composition. Hence, only part of the total enthalpy and entropy change in step 2 occurs at the eutectic temperature (melting and mixing of the eutectic), while the remainder is spread out over the temperature range from the eutectic to the liquidus: i.e., between points 5 and 6 in Figure 3. This also has an effect on the integrations in step 3 over the same temperature range as the fraction and the composition of the liquid changes. In terms of enthalpy, all of this is captured in the integration of the endotherm to obtain the total enthalpy. In terms of entropy, however, there will be errors emanating from assuming that the total heat transfer for the melting and mixing occurs at the eutectic temperature and from the heat capacity integration.

Through integration of the main peak and the residual tail of the thermograms of the physical mixture, it is estimated that approximately 85% of the total enthalpy change of the event is derived from the eutectic melting and 15% from the residual melting of SMT. As the difference in temperature between the eutectic and the liquidus compositions (points 4 and 5 in Figure 3) is estimated to be below 10 K, the error is expected to be fairly limited. An estimate of the maximum possible magnitude of this error can be obtained by comparing the entropy value obtained with the current assumption (in Table 2) with the value that would be obtained by assuming that all the SMT in excess of the eutectic composition melts and mixes with the solution at the temperature in point 5, i.e. assuming that all the heat transfer for this residual part of the melting and mixing process takes place at the highest possible temperature, and integrating the heat capacities accordingly. The resulting maximum estimate of the error in the entropy term is  $0.4 \text{ kJ mol}^{-1}$ , or 8% in relative terms. As the heat transfer occurs gradually over the estimated 9.4 K between points 4 and 5, the real error will likely be smaller. Please note that this error is in addition to the uncertainties given in Table 2. For comparison, the ideal entropy term for random equimolar mixing of two components,  $RT \ln 2$ , is equal to  $1.7 \text{ kJ mol}^{-1}$ .

$\Delta_{\text{form}}G_{\text{C}}$ ,  $\Delta_{\text{form}}H_{\text{C}}$ , and  $T\Delta_{\text{form}}S_{\text{C}}$  are shown as functions of  $T$  in Figure 5. As shown in the figure, the estimated Gibbs energy for cocrystal formation is negative throughout the entire temperature interval evaluated: i.e., the cocrystal is stable in relation to the physical mixture and formation of the cocrystal from its solid components is thermodynamically favorable. This stability increases (the Gibbs energy term becomes increasingly negative) with increasing temperature, from a value of  $-1.7 \text{ kJ mol}^{-1}$  at room temperature to a value of  $-7.0 \text{ kJ mol}^{-1}$  at the melting point of the cocrystal. The enthalpic term is strongly positive, however, signifying that cocrystal formation is an endothermic process and that the total cost of

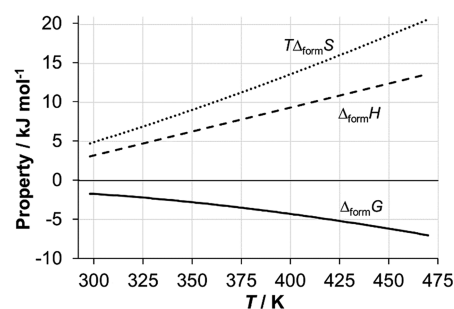


Figure 5.  $\Delta_{\text{form}}G$ ,  $\Delta_{\text{form}}H$ , and  $T\Delta_{\text{form}}S$  vs  $T$  for the 1:1 cocrystal.

breaking A–A and B–B bonds between the pure components exceeds the gain of forming A–B bonds in the cocrystal lattice. The process of cocrystal formation is thus driven by the accompanying increase in entropy. This has been suggested to be a more common situation than previously understood.<sup>24,25</sup>

Since the enthalpy change is positive, it may be assumed that with further decrease in temperature, and accompanying diminishing of the entropy term, cocrystal formation will at some point become unfavorable. This would be somewhat analogous to the case of enantiotropic polymorphism, where a spontaneous, endothermic transformation on heating indicates the existence of a transition point at a lower temperature. As shown in Figure 5, however, such a transition point is likely to be located at a very low temperature. For comparison, the reported 1:1 cocrystal between celecoxib and nicotinamide has a confirmed transition point located between 4 and 25 °C.<sup>24</sup>

On comparison of the numerical values of the enthalpy and entropy terms obtained for the five steps of the thermodynamic cycle at room temperature (Table 2), a few noteworthy observations can be made. First of all, the total enthalpy and entropy terms clearly are small sums of large numbers, with all five steps contributing with numbers of the same order of magnitude. With regard to the enthalpy terms, steps 2 and 4 are responsible for the major part of the total enthalpy for cocrystal formation (86%) with the contributions from heat capacity (steps 1, 3, and 5) to a large extent canceling out, as expected. With regard to the entropy terms, however, the contributions from the heat capacity terms are fairly significant (35% of the magnitude of the sum of steps 2 and 4), and with opposite sign, partially counteracting the large sum of contributions from steps 2 and 4. In terms of Gibbs energy, the sum of steps 2 and 4, corresponding to  $\Delta_{\text{form}}G_{\text{C}}$  without accounting for heat capacity differences, is  $-2.9 \text{ kJ mol}^{-1}$  (standard uncertainty of 0.25) while the component of  $\Delta_{\text{form}}G_{\text{C}}$  stemming purely from heat capacity differences between the phases is  $+1.2 \text{ kJ mol}^{-1}$  (42% of the magnitude of the sum of steps 2 and 4, albeit with a fairly large standard uncertainty of 0.63). For  $\Delta_{\text{form}}G_{\text{C}}$ , neglecting all contributions from heat capacity results in an error of 71%. This stresses the importance of including heat capacity terms in estimating thermodynamic properties.

In a previous contribution<sup>33</sup> we estimated values for the thermodynamic functions of formation of the 1:1 SMT-SA cocrystal using solubility data in acetonitrile. Using eq 5 and data in acetonitrile (a congruently dissolving system), the value of  $\Delta_{\text{form}}G_{\text{C}}$  at 283 K was estimated as  $-5.7 \text{ kJ mol}^{-1}$ , becoming increasingly negative with increasing temperature. Using approximated solubility data in the solvents methanol and a 7/3 (v/v) DMSO/methanol mixture,  $\Delta_{\text{form}}G_{\text{C}}$  values at 283 K of  $-6.0$  and  $-6.8 \text{ kJ mol}^{-1}$  were obtained. The value of

$\Delta_{\text{form}}G_{\text{C}}$  at 283 K estimated using calorimetric data is  $-1.5 \text{ kJ mol}^{-1}$  (estimated uncertainty of  $\pm 1.2 \text{ kJ mol}^{-1}$  at the 95% confidence level). Hence, even when the uncertainties in the calorimetric determination emanating both from experimental factors and the necessary assumptions introduced are allowed for, the values of  $\Delta_{\text{form}}G_{\text{C}}$  obtained using solubility data are still larger in magnitude than the value obtained in the present work. A reasonable hypothesis is that a non-negligible part of the statistically significant difference is caused by the approximation of activities with concentrations in the solubility-based method. This approximation entails neglecting all dependence of the activity coefficient of each of the components on (i) the concentration of that particular component in the solution as well as (ii) the presence and concentration of the third component—the other cofomer. This is a common approximation, which may be expected to work well for systems forming solutions that are close to ideal but which could lead to significant errors for systems where the activity coefficients clearly deviate more from unity. However, it is notable that despite the deviation between the sets of absolute values of the thermodynamic properties obtained with the two methods, the analyses agree qualitatively with respect to the main findings: viz., (i) that the formation of the cocrystal from the pure components is thermodynamically favorable, (ii) that the thermodynamic stability of the cocrystal increases with increasing temperature, and (iii) that the cocrystal formation is an entropy-driven process.

Zhang et al.<sup>19</sup> found that, for almost all cocrystals containing nicotinamide, the molecular volume in the crystal lattice is larger than the sum of the volumes occupied by the cofomer molecules in their respective crystal lattice. Perlovich<sup>18</sup> investigated the connection between this increase in molecular volume and the entropy for cocrystal formation, and found fair, positive correlations for cocrystals of several APIs with various cofomers. If one molecule of cocrystal C is defined as one molecule of A and one molecule of B, the increase in molecular volume becomes

$$\Delta_{\text{form}}V_{\text{C}} = \frac{V_{\text{cell,C}}}{Z_{\text{C}}} - \left( \frac{V_{\text{cell,A}}}{Z_{\text{A}}} + \frac{V_{\text{cell,B}}}{Z_{\text{B}}} \right) \quad (11)$$

where  $V_{\text{cell}}$  denotes the unit cell volume and  $Z$  the number of molecules in the unit cell. For the present cocrystal system, using data from the Cambridge Structural Database for the structures with refcodes SLFNMD10 (SMT), SALIAC12 (SA) and GEYSAE (the cocrystal), the increase in molecular volume upon cocrystal formation was calculated according to eq 11. No correction for thermal expansion is required, as the chosen structures were all determined at room temperature. For the 1:1 cocrystal, the increase in volume is  $+27.3 \text{ \AA}^3/\text{molecule}$ , corresponding to 6%. Given the positive  $T\Delta_{\text{form}}S_{\text{C}}$  term of  $4.8 \text{ kJ mol}^{-1}$  at 298 K, the 1:1 SMT-SA cocrystal behaves qualitatively like the systems in Perlovich's data set.<sup>18</sup> A comparison of the crystal structures reveals that the SMT molecule participates in additional hydrogen-bonding interactions in the cocrystal in comparison to that in its pure component structure. It is plausible that the additional hydrogen bonding could form part of the explanation why the cocrystal has a more open structure than the pure component crystals. Indeed, similar observations have been made for nicotinamide–mandelic acid cocrystals.<sup>23</sup>

**5.3. Quantifying the Gibbs Energy of Equimolar Mixing.** The Gibbs energy of fusion of a pure solid phase as a

function of  $T$ ,  $\Delta_{\text{fus}}G$ , can be experimentally estimated using DSC data.<sup>40</sup> This property is related to the activity of the pure solid phase, with the pure supercooled melt as the reference state, and hence to the activity of the respective phase in a saturated solution (often called the ideal solubility). The process of experimentally determining  $\Delta_{\text{fus}}G$  entails accurately measuring the melting temperature,  $T_{\text{m}}$ , the associated enthalpy of fusion,  $\Delta_{\text{fus}}H(T_{\text{m}})$ , and the specific heat capacities of both the solid and the melt as functions of  $T$ . The Gibbs energy for the process is  $\Delta_{\text{fus}}G = \Delta_{\text{fus}}H - T\Delta_{\text{fus}}S$ . If the heat capacities can be approximated as linear functions of temperature (eq 6), the enthalpy and entropy components become

$$\begin{aligned} \Delta_{\text{fus}}H(T) &= \Delta_{\text{fus}}H(T_{\text{m}}) + \int_{T_{\text{m}}}^T C_{\text{p}}^{\text{l}} dT + \int_T^{T_{\text{m}}} C_{\text{p}}^{\text{s}} dT = \\ &\Delta_{\text{fus}}H(T_{\text{m}}) + \left( \frac{k^{\text{l}} - k^{\text{s}}}{2} \right) (T^2 - T_{\text{m}}^2) + (m^{\text{l}} - m^{\text{s}})(T - T_{\text{m}}) \end{aligned} \quad (12)$$

$$\begin{aligned} \Delta_{\text{fus}}S(T) &= \Delta_{\text{fus}}S(T_{\text{m}}) + \int_{T_{\text{m}}}^T \frac{C_{\text{p}}^{\text{l}}}{T} dT + \int_T^{T_{\text{m}}} \frac{C_{\text{p}}^{\text{s}}}{T} dT = \\ &\frac{\Delta_{\text{fus}}H(T_{\text{m}})}{T_{\text{m}}} + (k^{\text{l}} - k^{\text{s}})(T - T_{\text{m}}) + (m^{\text{l}} - m^{\text{s}}) \ln \frac{T}{T_{\text{m}}} \end{aligned} \quad (13)$$

Combining the Gibbs energies of fusion of the three solid phases results in a value which can be interpreted as an estimate of  $\Delta_{\text{form}}G_{\text{C}}$  where contributions from equimolar liquid–liquid mixing of A and B are neglected:

$$\begin{aligned} \Delta_{\text{fus}}G_{\text{A}} + \Delta_{\text{fus}}G_{\text{B}} - \Delta_{\text{fus}}G_{\text{C}} &= G_{\text{A}}^{\text{l}} - G_{\text{A}}^{\text{s}} + G_{\text{B}}^{\text{l}} - G_{\text{B}}^{\text{s}} + G_{\text{C}}^{\text{s}} - G_{\text{C}}^{\text{l}} \\ &= \Delta_{\text{form}}G_{\text{C}} - \Delta_{\text{mix}}G \end{aligned} \quad (14)$$

On rearrangement, an expression is obtained that allows the Gibbs energy of mixing of equimolar amounts of melts of pure A and pure B to be obtained from the Gibbs energies for cocrystal formation and fusion:

$$\Delta_{\text{mix}}G = \Delta_{\text{form}}G_{\text{C}} - \Delta_{\text{fus}}G_{\text{A}} - \Delta_{\text{fus}}G_{\text{B}} + \Delta_{\text{fus}}G_{\text{C}} \quad (15)$$

The expression can be evaluated at any temperature, and can be used analogously for the enthalpy and entropy components. For the 1:1 SMT-SA cocrystal, estimated values of the mixing terms at 298 K are  $\Delta_{\text{mix}}G = -1.7 \text{ kJ mol}^{-1}$ ,  $\Delta_{\text{mix}}H = -0.9 \text{ kJ mol}^{-1}$ , and  $T\Delta_{\text{mix}}S = 0.8 \text{ kJ mol}^{-1}$ . In other words, liquid mixing of equal amounts of SMT and SA is an important, weakly exothermic process at room temperature. Formation of the cocrystal from its solid components is an endothermic process with a large entropy increase, however.

Direct experimental measurement of the Gibbs energy of mixing of the two supercooled melts A and B is nontrivial. For an ideal mixture, the enthalpy of mixing is zero, and the Gibbs energy is given by the entropy of complete random mixing of equal parts of A and B molecules with identical size and geometry,  $\Delta_{\text{mix}}^{\text{id}}S$ :

$$\Delta_{\text{mix}}^{\text{id}}G = -T\Delta_{\text{mix}}^{\text{id}}S = -RT \ln 2 \quad (16)$$

The ideal Gibbs energy of mixing amounts to  $-1.7 \text{ kJ mol}^{-1}$  at room temperature. The ideal entropy term for random

equimolar mixing ( $1.7 \text{ kJ mol}^{-1}$ ) is somewhat higher than the entropy of mixing term for the 1:1 SMT-SA cocrystal. The results suggest that the liquid mixture could feature some degree of order in comparison to a random mixture, especially given the fact that molecular size differences are expected to result in a positive excess entropy contribution.<sup>41</sup> Because of compensation from the negative enthalpy term, however, the Gibbs energy of mixing is almost identical with the ideal value. It is notable that, in spite of the fact that the solid cocrystal is an ordered 1:1 mixture, the entropy of cocrystal formation from pure solid cofomers significantly exceeds the entropy of mixing of an ideal liquid.

If the thermodynamic analysis is carried out neglecting all heat capacity terms, estimated values of the mixing terms at 298 K become  $\Delta_{\text{mix}}G = -2.4 \text{ kJ mol}^{-1}$ ,  $\Delta_{\text{mix}}H = 0.4 \text{ kJ mol}^{-1}$ , and  $T\Delta_{\text{mix}}S = 2.9 \text{ kJ mol}^{-1}$ . The corresponding values for cocrystal formation at 298 K, neglecting heat capacity terms, become  $\Delta_{\text{form}}G_{\text{C}} = -2.9 \text{ kJ mol}^{-1}$ ,  $\Delta_{\text{form}}H_{\text{C}} = 3.3 \text{ kJ mol}^{-1}$ , and  $T\Delta_{\text{form}}S_{\text{C}} = 6.2 \text{ kJ mol}^{-1}$ .

## 6. CONCLUSIONS

The present study demonstrates how calorimetry-based values of the Gibbs energy, enthalpy, and entropy of cocrystal formation from the pure solid cofomers can be obtained. The Gibbs energy, enthalpy, and entropy for the formation of the 1:1 cocrystal between sulfamethazine and salicylic acid are reported as functions of temperature. The Gibbs energy term is negative from room temperature to the cocrystal melting point, becoming increasingly negative with increasing temperature, showing that the cocrystal is the stable form in a 1:1 mixture of the cofomers throughout the temperature interval. At room temperature, the Gibbs energy term is estimated as  $-1.7 \text{ kJ mol}^{-1}$ . Both the enthalpic and entropic component terms are positive, at 298 K estimated as 3.1 and 4.8  $\text{kJ mol}^{-1}$ , respectively, showing that cocrystal formation is endothermic and is driven by the entropy increase. Cocrystal formation is associated with a 6% increase in molecular volume. The Gibbs energy, enthalpy, and entropy of fusion of the respective pure solid phases have been determined and used to estimate the thermodynamic functions of liquid mixing of equimolar amounts of cofomer melts. Equimolar cofomer mixing in the liquid state is a weakly exothermic process at room temperature, with the Gibbs energy of mixing estimated to  $-1.7 \text{ kJ mol}^{-1}$ , very close to the ideal value.

## ■ ASSOCIATED CONTENT

### Supporting Information

The Supporting Information is available free of charge at <https://pubs.acs.org/doi/10.1021/acs.cgd.9b01253>.

Experimental heat capacity data, XRPD of solid materials, TGA, and uncertainty analysis (PDF)

## ■ AUTHOR INFORMATION

### Corresponding Author

Michael Svård – Department of Chemical Engineering, KTH Royal Institute of Technology, SE-10044 Stockholm, Sweden; Synthesis and Solid State Pharmaceutical Centre, Department of Chemical and Environmental Science, Bernal Institute, University of Limerick, Castletroy, Ireland; [orcid.org/0000-0002-6647-3308](https://orcid.org/0000-0002-6647-3308); Email: [micsva@kth.se](mailto:micsva@kth.se)

## Authors

Dipali Ahuja – Synthesis and Solid State Pharmaceutical Centre, Department of Chemical and Environmental Science, Bernal Institute, University of Limerick, Castletroy, Ireland;

[orcid.org/0000-0003-0449-6632](https://orcid.org/0000-0003-0449-6632)

Åke C. Rasmuson – Department of Chemical Engineering, KTH Royal Institute of Technology, SE-10044 Stockholm, Sweden; Synthesis and Solid State Pharmaceutical Centre, Department of Chemical and Environmental Science, Bernal Institute, University of Limerick, Castletroy, Ireland;

[orcid.org/0000-0003-1790-2310](https://orcid.org/0000-0003-1790-2310)

Complete contact information is available at: <https://pubs.acs.org/10.1021/acs.cgd.9b01253>

## Notes

The authors declare no competing financial interest.

## ■ ACKNOWLEDGMENTS

This publication has emanated from research conducted with the financial support of the Swedish Research Council (Grants 2015-5240 and 2019-5059) and the Synthesis and Solid State Pharmaceutical Centre, which is financed by a research grant from Science Foundation Ireland (SFI) cofunded under the European Regional Development Fund (Grant 12/RC/2275).

## ■ REFERENCES

- (1) Steed, J. W. The role of co-crystals in pharmaceutical design. *Trends Pharmacol. Sci.* **2013**, *34*, 185.
- (2) Blagden, N.; de Matas, M.; Gavan, P. T.; York, P. Crystal engineering of active pharmaceutical ingredients to improve solubility and dissolution rates. *Adv. Drug Delivery Rev.* **2007**, *59*, 617.
- (3) Jayasankar, A.; Roy, L.; Rodríguez-Hornedo, N. Transformation pathways of cocrystal hydrates when cofomer modulates water activity. *J. Pharm. Sci.* **2010**, *99*, 3977.
- (4) *Regulatory classification of pharmaceutical co-crystals - guidance for industry*; Food and Drug Administration - Center for Drug Evaluation and Research (CDER): 2018.
- (5) Grothe, E.; Meeke, H.; Vlieg, E.; Ter Horst, J. H.; De Gelder, R. Solvates, salts, and cocrystals: a proposal for a feasible classification system. *Cryst. Growth Des.* **2016**, *16*, 3237.
- (6) Trask, A. V.; Jones, W. Crystal engineering of organic cocrystals by the solid-state grinding approach. In *Organic Solid State Reactions*; Toda, F., Ed.; Springer Berlin Heidelberg: Berlin, Heidelberg, 2005; p 41.
- (7) Chiarella, R. A.; Davey, R. J.; Peterson, M. L. Making co-crystals: the utility of ternary phase diagrams. *Cryst. Growth Des.* **2007**, *7*, 1223.
- (8) Shan, N.; Toda, F.; Jones, W. Mechanochemistry and co-crystal formation: effect of solvent on reaction kinetics. *Chem. Commun.* **2002**, 2372.
- (9) Friscic, T.; Fabian, L.; Burley, J. C.; Jones, W.; Motherwell, W. D. S. Exploring cocrystal-cocrystal reactivity via liquid-assisted grinding: the assembling of racemic and dismantling of enantiomeric cocrystals. *Chem. Commun.* **2006**, 5009.
- (10) Vishweshwar, P.; McMahan, J. A.; Peterson, M. L.; Hickey, M. B.; Shattock, T. R.; Zaworotko, M. J. Crystal engineering of pharmaceutical co-crystals from polymorphic active pharmaceutical ingredients. *Chem. Commun.* **2005**, 4601.
- (11) Patil, S. P.; Modi, S. R.; Bansal, A. K. Generation of 1:1 carbamazepine:nicotinamide cocrystals by spray drying. *Eur. J. Pharm. Sci.* **2014**, *62*, 251.
- (12) McIntosh, J.; Robinson, R. H. M.; Selbie, F. R. Acridine-sulphonamide compounds as wound antiseptics: clinical trials of flavazole. *Lancet* **1945**, *246*, 97.
- (13) Ghosh, S.; Bag, P. P.; Reddy, C. M. Co-crystals of sulfamethazine with some carboxylic acids and amides: co-former

assisted tautomerism in an active pharmaceutical ingredient and hydrogen bond competition study. *Cryst. Growth Des.* **2011**, *11*, 3489.

(14) Basak, A. K.; Mazumdar, S. K.; Chaudhuri, S. Structure of sulphamethazine [4-amino-N-(4,6-dimethyl-2-pyrimidinyl)-benzenesulphonamide], C<sub>12</sub>H<sub>14</sub>N<sub>4</sub>O<sub>2</sub>S. *Acta Crystallogr., Sect. C: Cryst. Struct. Commun.* **1983**, *39*, 492.

(15) Caira, M. R. Sulfa drugs as model cocrystal formers. *Mol. Pharmaceutics* **2007**, *4*, 310.

(16) Patel, U.; Haridas, M.; Singh, T. P. Structure of the 1:1 complex between 4-amino-N-(4,6-dimethyl-2-pyrimidinyl)-benzenesulfonamide (sulfadimidine) and 2-hydroxybenzoic acid (salicylic acid). *Acta Crystallogr., Sect. C: Cryst. Struct. Commun.* **1988**, *44*, 1264.

(17) Surov, A. O.; Solanko, K. A.; Bond, A. D.; Bauer-Brandl, A.; Perlovich, G. L. Cocrystals of the antiandrogenic drug bicalutamide: screening, crystal structures, formation thermodynamics and lattice energies. *CrystEngComm* **2016**, *18*, 4818.

(18) Perlovich, G. L. Two-component molecular crystals: relationship between the entropy term and the molecular volume of co-crystal formation. *CrystEngComm* **2018**, *20*, 3634.

(19) Zhang, S.-W.; Harasimowicz, M. T.; de Villiers, M. M.; Yu, L. Cocrystals of nicotinamide and (R)-mandelic acid in many ratios with anomalous formation properties. *J. Am. Chem. Soc.* **2013**, *135*, 18981.

(20) Zhang, S.; Chen, H.; Rasmuson, Å. C. Thermodynamics and crystallization of a theophylline–salicylic acid cocrystal. *CrystEngComm* **2015**, *17*, 4125.

(21) Oliveira, M. A.; Peterson, M. L.; Davey, R. J. Relative enthalpy of formation for co-crystals of small organic molecules. *Cryst. Growth Des.* **2011**, *11*, 449.

(22) Issa, N.; Karamertzanis, P. G.; Welch, G. W. A.; Price, S. L. Can the formation of pharmaceutical cocrystals be computationally predicted? I. Comparison of lattice energies. *Cryst. Growth Des.* **2009**, *9*, 442.

(23) Zhang, S.-W.; Kendrick, J.; Leusen, F. J. J.; Yu, L. Cocrystallization with nicotinamide in two conformations lowers energy but expands volume. *J. Pharm. Sci.* **2014**, *103*, 2896.

(24) Zhang, S.-W.; Brunskill, A. P. J.; Schwartz, E.; Sun, S. Celecoxib–nicotinamide cocrystal revisited: can entropy control cocrystal formation? *Cryst. Growth Des.* **2017**, *17*, 2836.

(25) Perlovich, G. L. Two-component molecular crystals: evaluation of the formation thermodynamics based on melting points and sublimation data. *CrystEngComm* **2017**, *19*, 2870.

(26) Schartman, R. R. On the thermodynamics of cocrystal formation. *Int. J. Pharm.* **2009**, *365*, 77.

(27) Zhang, S.; Rasmuson, Å. C. Thermodynamics and crystallization of the theophylline–glutaric acid cocrystal. *Cryst. Growth Des.* **2013**, *13*, 1153.

(28) Zhang, S.; Rasmuson, Å. C. The theophylline–oxalic acid cocrystal system: solid phases, thermodynamics and crystallisation. *CrystEngComm* **2012**, *14*, 4644.

(29) Evora, A. O. L.; Bernardes, C. E. S.; Piedade, M. F. M.; Conceição, A. C. L.; Minas da Piedade, M. E. Energetics of glycine cocrystal or salt formation with two regioisomers: fumaric acid and maleic acid. *Cryst. Growth Des.* **2019**, *19*, 5054.

(30) Nehm, S. J.; Rodríguez-Spong, B.; Rodríguez-Hornedo, N. Phase solubility diagrams of cocrystals are explained by solubility product and solution complexation. *Cryst. Growth Des.* **2006**, *6*, 592.

(31) Perlovich, G. L. Thermodynamic characteristics of cocrystal formation and melting points for rational design of pharmaceutical two-component systems. *CrystEngComm* **2015**, *17*, 7019.

(32) Braun, D. E.; Ardid-Candel, M.; D'Oria, E.; Karamertzanis, P. G.; Arlin, J.-B.; Florence, A. J.; Jones, A. G.; Price, S. L. Racemic naproxen: a multidisciplinary structural and thermodynamic comparison with the enantiopure form. *Cryst. Growth Des.* **2011**, *11*, 5659.

(33) Ahuja, D.; Svärd, M.; Rasmuson, Å. C. Investigation of solid–liquid phase diagrams of the sulfamethazine–salicylic acid co-crystal. *CrystEngComm* **2019**, *21*, 2863.

(34) Bacon, G. E.; Jude, R. J. Neutron-diffraction studies of salicylic acid and  $\alpha$  resorcinol. *Z. Krist. - Cryst. Mater.* **1973**, *138*, 19.

(35) Nordström, F. L.; Rasmuson, Å. C. Solubility and melting properties of salicylic acid. *J. Chem. Eng. Data* **2006**, *51*, 1668.

(36) Neau, S. H.; Bhandarkar, S. V.; Hellmuth, E. W. Differential molar heat capacities to test ideal solubility estimations. *Pharm. Res.* **1997**, *14*, 601.

(37) Svärd, M.; Rasmuson, Å. C. (Solid + liquid) solubility of organic compounds in organic solvents – correlation and extrapolation. *J. Chem. Thermodyn.* **2014**, *76*, 124.

(38) Neau, S. H.; Flynn, G. L. Solid and liquid heat capacities of n-alkyl para-aminobenzoates near the melting point. *Pharm. Res.* **1990**, *07*, 1157.

(39) Yamashita, H.; Hirakura, Y.; Yuda, M.; Teramura, T.; Terada, K. Detection of cocrystal formation based on binary phase diagrams using thermal analysis. *Pharm. Res.* **2013**, *30*, 70.

(40) Svärd, M.; Valavi, M.; Khamar, D.; Kuhs, M.; Rasmuson, Å. C. Thermodynamic stability analysis of tolbutamide polymorphs and solubility in organic solvents. *J. Pharm. Sci.* **2016**, *105*, 1901.

(41) Lichtenthaler, N. R.; Abrams, D. S.; Prausnitz, J. M. Combinatorial entropy of mixing for molecules differing in size and shape. *Can. J. Chem.* **1973**, *51*, 3071.